International Journal of Fatigue 23 (2001) 655–670

International Journal of Fatigue

www.elsevier.com/locate/ijfatigue

Crack bridging model for fibre reinforced concrete under fatigue tension

Jun Zhang [a,*], Henrik Stang [b], Victor C. Li [c]

[a] *Department of Civil Engineering, Tsinghua University, Beijing 100084, People's Republic of China*
[b] *Department of Structural Engineering and Materials, Technical University of Denmark, DK2800 Lyngby, Denmark*
[c] *Advanced Civil Engineering Materials Research Laboratory, Department of Civil and Environmental Engineering, University of Michigan, Ann Arbor, MI 48109, USA*

Received 4 April 2000; received in revised form 11 March 2001; accepted 20 April 2001

Abstract

Recent theoretical investigations have shown that the rate of fatigue crack growth in fibre reinforced cement-based composites is strongly dependent on the cyclic crack bridging law of the materials. Thus, the basic understanding on crack bridging mechanics is very important and can provide a means of significant improvement of the fatigue performance of fibre reinforced concrete (FRC) structures. In this paper, a cyclic crack bridging model including bond between fibre and matrix degradation for FRC is developed. The model is based on the assumption that the frictional dependent bond strength is gradually reduced due to the interface degradation during fibre pull-out and slip-back. The model predictions are compared with the test results on FRC materials under uniaxial fatigue tension. Good correlation between experiments and theoretical calculations is found.

Keywords: Fibre reinforced concrete; Fatigue tension; Crack bridging; Model; Bond degradation

1. Introduction

Incorporation of steel or other fibres in concrete has been found to improve several of its properties, primarily cracking resistance, impact and wear resistance and ductility. For this reason fibre reinforced concrete (FRC) is now being used in increasing amounts in structures such as airport pavements, highway pavements, bridge decks, machine foundations and storage tanks. Thus, the fatigue performance of FRC materials has to be investigated due to the described reasons. The history of investigation of the fatigue of FRC is not very long. Experimental evaluations of this behaviour have been carried out in recent years [1–4]. Most of fatigue life prediction and design of FRC structures have been conducted mainly through an empirical approach. This type of approach requires time-consuming test data collection and processing for a broad range of design cases which, in principle, is not applicable to other design cases. Therefore, a mechanism based fatigue model that is capable of both predicting the fatigue life for a given FRC structure and designing a FRC material for a given fatigue life has to be constructed.

Recent theoretical studies [5–10] have revealed that the rate of fatigue crack growth in a number of different materials, which exhibit crack bridging, is highly dependent on the crack bridging law governing the zone behind the matrix crack and on the law governing the degradation of the crack bridging with the number of load cycles. Thus, the study on the cyclic crack bridging behaviour of FRC materials in both experiments and theoretical modelling becomes fundamental work in order to design and improve FRC structures with fatigue performance requirements. An experimental study on the bridging behaviour of FRCs under uniaxial fatigue tension has been carried out by Zhang et al. [10]. The experimental results show that the bridging stress degrades with the number of load cycles and it can be assumed that the degradation of the bridging stress is related primarily to degradation of the interfacial bond between fibre and matrix, even though other mechanisms

* Corresponding author. Tel.: +86-10-62785835; fax: +86-10-62771132.
E-mail address: junz@mail.tsinghua.edu.cn (J. Zhang).

0142-1123/01/$ - see front matter
PII: S0142-1123(01)00041-X

can be present. Such mechanisms include fatigue failure of the fibres in tension/bending during crack opening or fatigue in the fibres in compression/bending during crack closing and subsequent fibre buckling as non-metallic fibres are applied [11]. The purpose of the present paper is to derive a semi-analytical crack bridging model which is able to predict the cyclic crack bridging behaviour of a composite, especially for FRC, based on the properties of fibres, matrix and fibre/matrix interface. In this modelling work, first a theoretical model of a single fibre pull-out under cyclic load under the effect of bond degradation is developed. An interfacial bond degradation law accounting for accumulated damage on fibre/matrix interfaces during cyclic loading is proposed. Meanwhile, an empirical cyclic aggregate bridging model with bridging degradation is given. Then, this single fibre pull-out model and the aggregate bridging model are employed to derive the total crack bridging accounting for random fibre orientation, embedded length and fibre snubbing effect [12], as well as the Cook–Gordon debonding effect [13]. Finally, the model predictions are compared with the experiments and a good agreement between theoretical predictions and experimental results is obtained.

2. Derivation of the model

The whole contribution to fatigue cycle dependent crack bridging $\sigma(N, W)$ in fibre reinforced concrete is composed of two parts, aggregate bridging, $\sigma_a(N, W)$, and fibre bridging, $\sigma_f(N, W)$, i.e.

$$\sigma(N, W)=\sigma_f(N, W)+\sigma_a(N, W) \tag{1}$$

where N is the load cycle and W is the crack width, including the Cook–Gordon debonding effect.

2.1. Fibre bridging stress

The total contribution of fibres to the bridging stress is predicted by computing the traction transmitted across the matrix crack by integrating the force contributions from those individual fibres which, at the given crack opening, are still crossing the crack plane. To calculate the total force transmitted across the matrix crack, it is then necessary to analyse the bridging force P carried by a single fibre. Before carrying out the analysis of a single fibre pull-out under cyclic load, some basic assumptions will be given.

- The fibres are three-dimensional randomly distributed in location and orientation.
- Both fibres and matrix are linearly elastic until failure.
- The effect of Poisson's ratio of fibre on the pull-out response is neglected.
- When fibre is loaded, the bond between fibre and matrix will fail along a part of the fibre/matrix interface, giving rise to what is called a debonded zone. Fibre surface roughness and matrix shrinkage induce a shear stress, so-called bond strength τ along the debonded interface.
- The bond between fibre and matrix is purely frictional and mechanical, as the elastic shear bond stress is neglected.
- Before full debonding of all fibres, the bond strength is a constant, and after that, it is a function of fibre-end slippage δ according to the event that the interfacial bond hardens with slippage [14] or weakens with slippage [14,15]. A convenient polynomial form which is employed previously and appears to describe the experimental pull-out data reasonable well [16] is used in current work, i.e.

$$\begin{aligned} &\tau=\tau_0 && \text{for } \delta\le\delta^* \\ &\tau=\tau_0+a_1\delta+a_2\delta^2 && \text{for } \delta>\delta^* \end{aligned} \tag{2}$$

where δ^* is the fibre-end slippage corresponding to full debonding of all fibres. It is given by

$$\delta^*=\frac{\tau L_f^2}{2(1+\eta)E_f d_f} \tag{3}$$

where $\eta=V_fE_f/V_mE_m$, and E_f, V_f and E_m, V_m, are the Young's modulus and volume fractions of fibre and matrix, respectively; L_f and d_f are the fibre length and diameter; and a_1, a_2 are two empirical constants which may be determined from single fibre pull-out tests. Here, the fibre-end refers to the end of the fibre exit.

2.1.1. Bridging force of a single fibre under cyclic pull-out load

Now consider an isolated fibre with a round cross section, diameter d_f, and an embedded length L being stretched out from a matrix cylinder by a cyclic force P with a constant amplitude A between maximum and minimum fibre-end slippage values, δ_{max} and δ_{min} (or crack width w_{max} and w_{min} if both segments are included), corresponding to loads P_{max} and P_{min}. The load procedures include first loading period ($0\rightarrow\delta_{max}$), unloading period ($\delta_{max}\rightarrow\delta_{min}$) and reloading period ($\delta_{min}\rightarrow\delta_{max}$), as shown in Fig. 1. The fibre pull-out procedure can be divided into debonding stage and pull-out stage by fibre exit–end slippage value, δ_{fd}, which corresponds to the displacement at which full debonding is completed. It is given by

$$\delta_{fd}=\frac{2\tau L^2}{(1+\eta)E_f d_f} \tag{4}$$

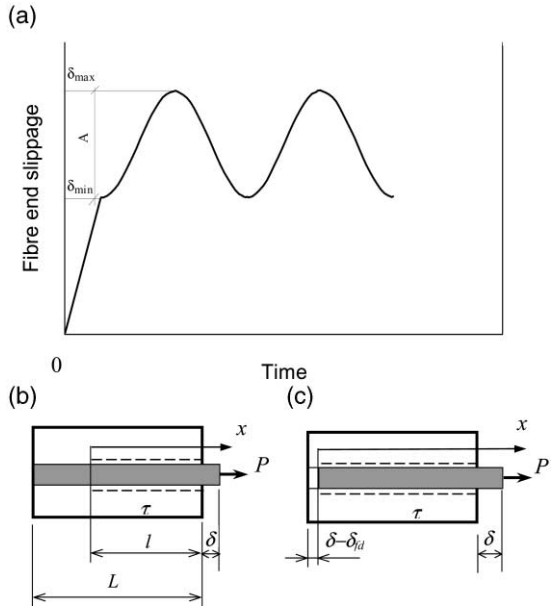

Fig. 1. Single fibre pull-out under deformation controlled cyclic load, deformation-time diagram (a) and schematic fiber stages of debonding (b) and pullout (c).

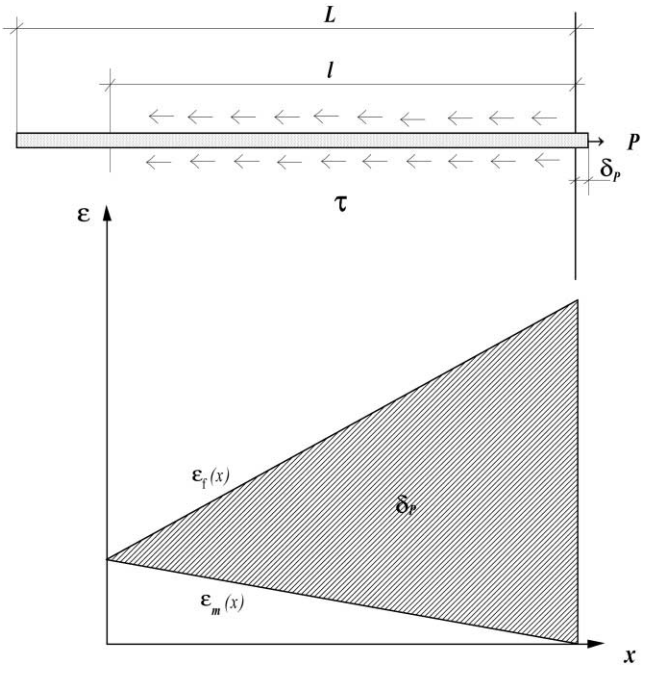

Fig. 2. Debonding period, first loading case.

2.1.1.1. Debonding period ($0<\delta<\delta_{fd}$)

1. First loading case ($0\rightarrow\delta_{max}$). With pull-out load increasing, the fibre/matrix interface undergoes a frictional debonding procedure. The debonding zone is gradually extended with the increase of load. Before debonding reaches the embedded end of the fibre (so-called debonding period), pull-out load P can be expressed as a function of fibre exit–end slippage δ as (Appendix A):

$$P(\delta)=\frac{\pi}{\sqrt{2}}[(1+\eta)E_f d_f^3\tau\delta]^{\frac{1}{2}} \tag{5}$$

When both segments are considered, the relation between load P and crack opening w ($w=2\delta$) is given by:

$$P(w)=\frac{\pi}{2}[(1+\eta)E_f d_f^3\tau w]^{\frac{1}{2}} \tag{6}$$

The bond and strain distribution along the debonding length in this stage is shown in Fig. 2. Graphically, the shaded area in the figure is equal to the fibre-end slippage value δ (see Appendix A).

2. Unloading case ($\delta_{max}\rightarrow\delta_{min}$). Unloading procedure starts when the fibre-end slippage reaches the maximum value δ_{max}. During this period, an assumption first proposed by Wu et al. [11] would be adapted. Wu et al. assume that a special zone is created where the same amount of interfacial stress acts in the reversed direction to resist fibres moving back into the matrix during unloading. The length of this reversed zone is a function of unloading magnitude as well as the initial bond strength. We further assume that when reloading starts again, the direction of the shear stress along the reversed zone will gradually change back and the size of this second reversal zone is dependent on the reloading level. The procedure of fibre pull-out (loading) and slip-back (unloading) will progressively smooth and wear out the interface between fibre and matrix which, in turn, leads to the frictional bond strength degradation.

For a general case, assume that a fibre has undergone N times of loading–unloading cycles. This fibre is now unloading to P from P_{max}. As a result, a reversed zone on bond stress of (l_N-x_1) is created along the debonding length l_N and the corresponding bond strengths in the different sections are τ and τ_N, as shown in Fig. 3. The pull-out force P is given by (Appendix A):

$$P(w,N)=(1+\eta)\pi d_f[2\tau_N x_1-\tau_N l_N+\Delta\tau_N x_{1,N}] \tag{7}$$

here $\tau_N=\tau-\Delta\tau_N$, $\Delta\tau_N$ is the total amount of bond strength reduction after N cycles of pull-out and slip-back. $x_{1,N}$ denotes the length of the unreversed zone of the last cycle. It is assumed that $\Delta\tau_N$ is a function of pull-out cycle as well as the amplitude of reversal slippage in the fibres during cyclic loading. Details on $\Delta\tau_N$ will be given in the following section. The length of the reversed zone x_1 can be related to crack width w by:

$$x_1=l_N-\left[\frac{1}{2\tau_N}\left(\tau l_N{}^2-\frac{d_f E_f}{4(1+\eta)}w-\Delta\tau_N(l_N-x_{1,N})^2\right)\right]^{\frac{1}{2}} \tag{8}$$

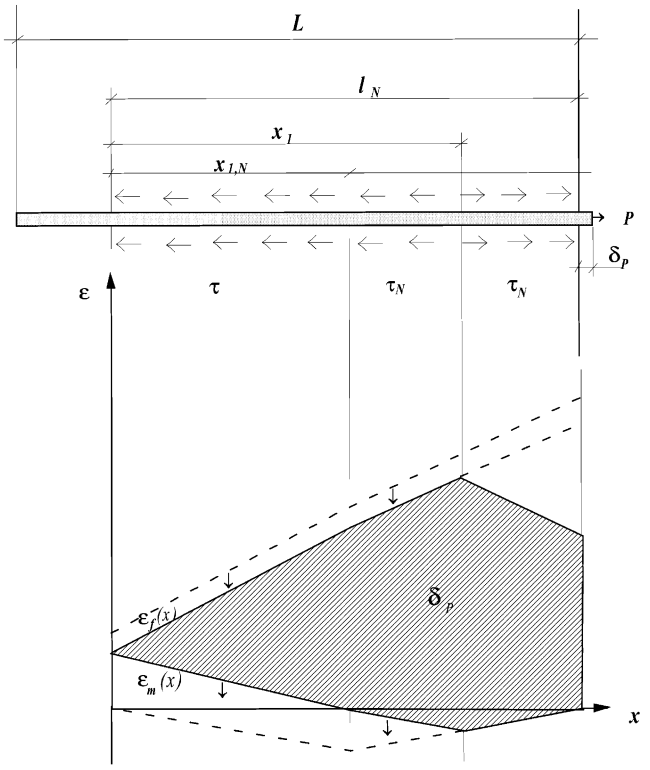

Fig. 3. Debonding period, unloading case with reverse shear interface.

when $P=P_{\min}$, $w=w_{\min}$ and $x_1=x_{1,N}$, thus from (8) we have:

$$x_{1,N}=l_N-\left[\frac{\tau}{\tau+\tau_N}l_N{}^2-\frac{d_fE_f}{4(\tau+\tau_N)(1+\eta)}w_{\min}\right]^{\frac{1}{2}} \tag{9}$$

Thus, using (8) and (9) for x_1 and $x_{1,N}$, respectively, in (7), the expression of P as a function of crack opening w and cycle N (the bond strength is a function of load cycles) can be obtained. Here it is noted that due to bond degradation during cyclic loading, to keep a constant fibre-end slippage value, a new debonding area is created in every cycle, thus the debonding length l_N will also be a function of load cycle. It can be updated in each cycle during numerical calculation.

3. Reloading case ($\delta_{\min}\rightarrow\delta_{\max}$). As stated above, during reloading, the direction of bond stress will change back again in part of the reversed zone and the size of this second reversal zone will depend upon the reloading level P. Thus, during reloading to P, the debonding length is divided into three sections, $x_{1,N}$, x_{21} and x_{22}, with bond strength τ, τ_N and τ_{N+1}, respectively, and with the specific bond directions, see Fig. 4. The pull-out force P is given by:

$$P(w,N)=(1+\eta)\pi d_f[\tau x_{1,N}+\tau_{N+1}(l_N-x_{1,N})-(\tau_N+\tau_{N+1})x_{21}] \tag{10}$$

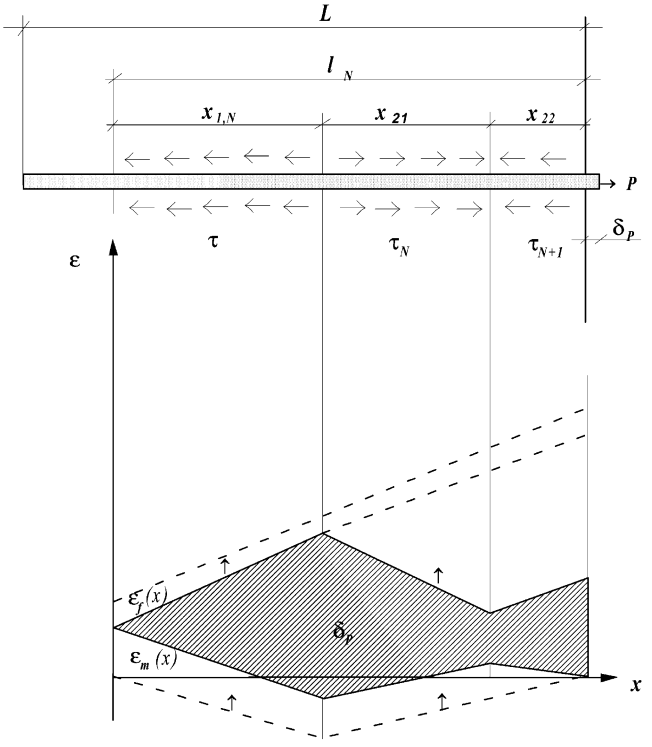

Fig. 4. Debonding period, reloading case reverse shear interface.

In this period, the debonding length l_N keeps the same value as in the last cycle. Similar to the unloading case, x_{21} can be related to crack opening w as:

$$x_{21}=(l_N-x_{1,N})-\frac{1}{\sqrt{\tau_N+\tau_{N+1}}}\left[\tau_N(l_N-x_{1,N})^2-2\tau x_{1,N}\left(l_N-\frac{1}{2}x_{1,N}\right)+\frac{d_fE_f}{4(1+\eta)}w\right]^{\frac{1}{2}} \tag{11}$$

Replacing x_{21} and $x_{1,N}$ with (11) and (9) in (10), the expression of reloading level P as a function of crack width w and cycle N can be obtained.

As mentioned above, due to the degradation of bond strength under cyclic tensile load, the maximum fibre-end slippage at reloading period will be less than the value of that in the last cycle if no new debonding area is developed. In order to arrive at the maximum fibre-end slippage $\delta_{\max}$, the fibre stretching-out process has to continue so that a new debonding area will be developed. Before fibre full debonding, the length of the stress degradation zone ($x_{2,N}$) remains constant during fibre continual pull-out, as shown in Fig. 5, and $x_{2,N}$ can be calculated by the following formula:

$$x_{2,N}=l_N-x_{1,N} \tag{12}$$

where $x_{1,N}$ is given by (7) and l_N is the debonding length of last cycle. The pull-out force P is given by:

$$P=(1+\eta)\pi d_f[\tau(l_{N+1}-x_{2,N})+\tau_{N+1}x_{2,N}] \tag{13}$$

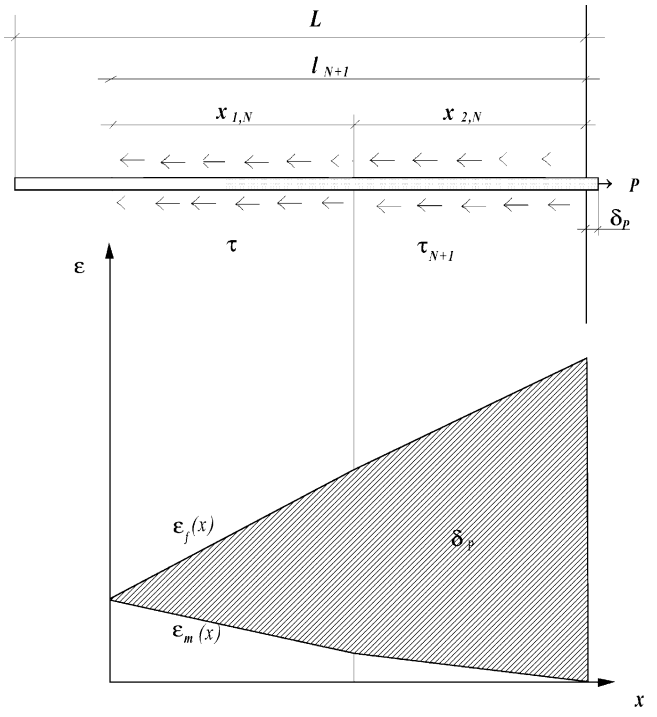

Fig. 5. Debonding period, fibre continue pull-out, reverse shear interface eliminated.

where

$$l_{N+1}=\left[\frac{\Delta\tau_{N+1}}{\tau}x_{2,N}^2+\frac{d_fE_fw}{4(1+\eta)\tau}\right]^{\frac{1}{2}} \quad (14)$$

here $\Delta\tau_{N+1}=\tau-\tau_{N+1}$. Replacing l_{N+1} with (14) in (13), we obtain:

$$P(w,N)=(1+\eta)\pi d_f\tau x_{2,N}\left[\left(\frac{E_fd_fw}{4(1+\eta)\tau x_{2,N}^2}+\frac{\Delta\tau_{N+1}}{\tau}\right)^{\frac{1}{2}}-\frac{\Delta\tau_{N+1}}{\tau}\right] \quad (15)$$

For simplicity, we assume that τ and τ_{N+1} remain constant during this period.

2.1.1.2. Fibre pull-out period ($\delta_{fd}<\delta<L+\delta_{fd}$) Complete debonding occurs when debonding length reaches its maximum value, the fibre embedded length. The fibre is assumed to be pulled out of the matrix without rupture. The complete relation of pull-out load and crack opening under cyclic pull-out load can be derived as follows.

1. First loading case ($0\rightarrow\delta_{max}$). In this period, the pull-out load can be approximated by:

$$P(\delta)=(1+\eta)\pi d_f\tau(L-\delta+\delta_{fd}) \quad (16)$$

where δ_{fd} is the fibre-end slippage produced by the maximum embedded length L which is given by (4). When both segments are considered ($\delta=w-\delta_{fd}$), we have:

$$P(w)=(1+\eta)\pi d_f\tau(L-w+w_{fd}) \quad (17)$$

where $2\delta_{fd}=w_{fd}$. This is the expression of bridging force P as a function of crack width w during fibre pull-out period.

2. Unloading case ($\delta_{max}\rightarrow\delta_{min}$). The assumptions described in the debonding period are applicable also in this stage. When pull-out load decreases to a certain value P from P_{max}, similar to the debonding period, P can be related to the total debonding length l_N and the fibre segment $x_{1,N}$ with unreversed shear by

$$P(w,N)=(1+\eta)\pi d_f[\tau_N(2x_1-l_N)+\Delta\tau_Nx_{1,N}] \quad (18)$$

Here $l_N=L-w_{max}+w_{fdN}$. The segment lengths x_1 and $x_{1,N}$ can be expressed by equations similar to (8) and (9), except that w and w_{min} must be replaced by $(w-w_{max}+w_{fdN})$ and $(w_{min}-w_{max}+w_{fdN})$, respectively. Thus

$$x_1=l_N-\left[\frac{1}{2\tau_N}\left(\tau l_N^2-\frac{d_fE_f}{4(1+\eta)}(w-w_{max}+w_{fdN})-\Delta\tau_N(l_N-x_{1,N})^2\right)\right]^{\frac{1}{2}} \quad (19)$$

and

$$x_{1,N}=l_N-\left[\frac{\tau}{\tau+\tau_N}l_N^2-\frac{d_fE_f}{4(\tau+\tau_N)(1+\eta)}(w_{min}-w_{max}+w_{fdN})\right]^{\frac{1}{2}} \quad (20)$$

where

$$w_{fdN}=\frac{4(1+\eta)}{d_fE_f}[\tau L^2-\Delta\tau_N(L-x_{1,N})] \quad (21)$$

It is noted that as $N=1$ (without bond degradation), $w_{fdN}=w_{fd}$. w_{fdN} will be updated cycle by cycle during numerical calculation. Similar to the case of debonding period, instead of x_1 and $x_{1,N}$ with Eqs. (19) and (20) in Eq. (18), we can get the model of unloading level P as a function of crack width w and load cycle N during fibre pull-out stage.

3. Reloading case ($\delta_{min}\rightarrow\delta_{max}$). The same as in debonding period, when reloading procedure starts, the embedded zone will be divided into three sections with different bond strengths and bond directions, see Fig. 4. At reloading P, we have

$$P(w,N)=(1+\eta)\pi d_f[\tau x_{1,N}+\tau_{N+1}(l_N-x_{1,N})-(\tau_N+\tau_{N+1})x_{21}] \quad (22)$$

x_{21} can also be expressed by an equation similar to (12), except replacing w with $(w-w_{max}+w_{fdN})$, i.e.

$$x_{21}=(l_N-x_{1,N})-\frac{1}{\sqrt{\tau_N+\tau_{N+1}}}\left[\tau_N(l_N-x_{1,N})^2 - 2\tau x_{1,N}\left(l_N-\frac{1}{2}x_{1,N}\right)+\frac{d_f E_f}{4(1+\eta)}(w-w_{max}+w_{fdN})\right]^{\frac{1}{2}} \quad (23)$$

Thus, the relationship between reloading level P and crack width w and cycle N is obtained. The same as in the debonding period, the maximum fibre exit–end slippage gradually decreases due to the interfacial degradation as with the same embedded length. Under deformation controlled cyclic pull-out load, to arrive at the maximum fibre slippage level, the fibre pull-out process has to continue after the maximum slippage has been reached as for the case without fibre pull-out, which corresponds to the point of x_{21} equal to zero. As the fibre pull-out continues, the bridging force is given by:

$$\begin{aligned} &P(w,N)=(1+\eta)\pi d_f[\tau_{N+1}(L-w+w_{fd})+\Delta\tau_{N+1}x_{1,N}] && \text{for } w\le l_N-x_{1,N}+w_{max}\\ &P(w,N)=(1+\eta)\pi d_f\tau(x_{1,N}-w+w_{fd}) && \text{for } w>l_N-x_{1,N}+w_{max}\end{aligned} \quad (24)$$

In the case of $\delta>\delta^*$, τ and τ_{N+1} can be obtained from the formulas given below. The undamaged bond strength τ is given by:

$$\tau(\delta)=\tau_0+a_1\delta+a_2\delta^2 \quad (25)$$

The damaged bond strength τ_{N+1} is given by:

$$\tau_{N+1}(\delta)=\tau_{0(N+1)}+a_1\delta+a_2\delta^2 \quad (26)$$

Using the condition $\tau_{N+1(\delta=\delta max)}=\tau_{0(N+1)}+a_1\delta_{max}+a_2\delta_{max}^2$ in (24):

$$\tau_{N+1}(\delta)=[\tau_{N+1}-a_1\delta_{max}-a_2\delta_{max}{}^2]+a_1\delta+a_2\delta^2 \quad (27)$$

with $\delta=w-\delta^*$.

2.1.1.3. Effect of the inclination angle In a composite with randomly distributed fibres, the fibre inclination angle, i.e. the orientation angle relative to the normal of the crack plane, can have any value between 0 and $\pi/2$. Various investigations have shown that a fibre inclined at an angle to the matrix crack plane leads to an increase in the bridging force. This is because when a fibre is pulled out at an angle to the crack plane there is an additional normal force acting on the surface of the fibre which is provided by the matrix wedge near the fibre exit point due to the change of direction in the fibre pull-out [12,17]. Thus, complementary friction develops between the fibre and matrix during fibre pull-out. The influence of this friction on the bridging force depends on the interfacial properties of the fibre and matrix and the inclination angle. According to Li et al. [12], this effect could be incorporated into the pull-out force by writing

$$P(w,\phi)=P(w,\phi=0)\,e^{f\phi} \quad (28)$$

where f is a coefficient of friction between fibre and matrix, the so-called snubbing coefficient that can be considered as one of the interfacial material parameters and which can be determined experimentally. For steel fibres in a concrete matrix, f lies somewhere between 0.5 and 1.0.

Under cyclic loading, the snubbing effect will gradually weaken due to the smoothing action along the fibre/matrix interfaces and the snubbing coefficient f can be related to bond strength at the Nth cycle τ_N through:

$$f_N=f\frac{\tau_N}{\tau} \quad (29)$$

where f and τ are the material parameters under monotonic load.

2.1.1.4. Interfacial bond degradation under cyclic pull-out loading It is well known that in materials which exhibit crack bridging, it is almost invariably the case that the bridging stress can be degraded by either time-dependent processes (creep, finite viscosity, chemical reaction with the environment, etc.) under monotonic loading conditions, or by cycle-dependent processes (debonding, attrition, work softing) under cyclic loading conditions [6]. In fibre reinforced cement based composites, bridging fibres also suffer from fatigue damages, exhibiting bridging stress degradation which is mainly due to the fibre/matrix interfacial damage or decay of the bond strength between fibre and matrix. Experimental observations on interfacial degradation under cyclic loading had been presented by Evans et al. [7] in fibre reinforced ceramics and by Zhang et al. [9,10] in fibre reinforced concrete.

In order to simulate crack bridging in FRC material under fatigue tension, an interfacial degradation model has to be developed first. Now, we assume: (1) the bond strength degradation only occurs along the stress-reversal zone; (2) the bond strength degradation is a function of load cycles N, initial bond strength τ_1 and the amplitude of fibre reversing slippage $\Delta\delta$ at the fibre exit point, i.e.

$$\frac{\Delta\tau_{N+1}}{\tau_1}=f(N,\Delta\delta_N)=k\Delta\delta_N \quad (30)$$

where $\tau_1=\tau$, $\Delta\tau_{N+1}$ is the bond strength reduction at the $(N+1)$th cycle, $\Delta\tau_{N+1}=\tau-\tau_{N+1}$, k is the normalized bond reduction coefficient which is time or cycle dependent, and $\Delta\delta_N$ is the amplitude of fibre reversing slippage at the Nth cycle. Considering load history effect on the bond degradation, for example in some cases the amplitude of fibre slippage may change during cyclic loading, it is reasonable to use the average amplitude of fibre reversing slippage as the representative value of $\Delta\delta_N$ when calculating $\Delta\tau_{N+1}$ with (30), i.e.

$$\Delta\delta_N=\frac{\sum_{i=1}^{N}\Delta\delta_i}{N}=\frac{\sum_{i=1}^{N}(\delta_{\max i}-\delta_{\min i})}{N} \tag{31}$$

where $\Delta\delta_i$ is the amplitude of fibre reversing slippage at the ith cycle. Under one-stage deformation controlled fatigue tensile load, Eq. (31) becomes $\Delta\delta_N=\delta_{\max}-\delta_{\min}$. For bond reduction factor k, it is assumed that k obeys a bi-linear function of log(N) as

$$\begin{aligned} k&=\beta_1\log(N+1) && \text{for } 1\le N\le N_0\\ k&=\beta_2\log(N+1)+(\beta_1-\beta_2)\log(N_0) && \text{for } N>N_0 \end{aligned} \tag{32}$$

where β_1, β_2 are the slopes in the k–log(N) curves in the two linear sections, respectively; see Fig. 6, which can be considered as a kind of material property that is controlled by the performance of the fibre/matrix interface. Replacing $\Delta\delta_N$ and k with (31) and (32) in (30), we obtain the bond strength degradation model under cyclic pull-out load as:

$$\begin{aligned} \frac{\Delta\tau_{N+1}}{\tau_1}&=\beta_1\log(N+1)\frac{\sum_{i=1}^{N}\Delta\delta_i}{N} && \text{for } 1\le N\le N_0\\ \frac{\Delta\tau_{N+1}}{\tau_1}&=[\beta_2\log(N+1)+(\beta_1-\beta_2)\log(N_0)]\frac{\sum_{i=1}^{N}\Delta\delta_i}{N} && \text{for } N>N_0 \end{aligned} \tag{33}$$

According to the present model, the interfacial bond decay is influenced by the number of load cycles N, initial bond strength τ_1, and loading history, i.e. the accumulated fibre slippage change $\Sigma\Delta\delta$.

2.1.2. Bridging stress in FRC under fatigue tensile load

As described previously, the total contribution of fibres to the bridging stress across a matrix crack can be obtained by integrating the contribution of the individual fibres, which at a given crack opening are still bridging the crack plane [18]. Thus, when the distributions of embedded length l and inclination angle ϕ are taken into consideration, for a composite with fibre volume fraction V_f of fibres length L_f and diameter d_f, the crack bridging contribution of fibres σ_f under fatigue load can be expressed as a function of crack width w and number of fatigue cycles N, i.e.

$$\sigma_f(w,N)=\frac{4V_f}{\pi d_f^2}\int_0^{\pi/2}\int_{w/2}^{L_f/2}P(w,N,\phi)p(\phi)p(L)\,\mathrm{d}\phi\,\mathrm{d}L \tag{34}$$

where $P(w, N, \phi)$ is the bridging force carried by a single fibre with an embedded length L and an orientation angle ϕ after N cycles. $p(\phi)$ and $p(L)$ are the probability density functions of the orientation angle and the embedded length. For three-dimensional uniformly distributed fibres, $p(L)=2/L_f$ and $p(\phi)=\sin\phi$.

1. Before full debonding of all fibres ($0\le w_{\max}\le w^*$, $w^*=2\delta^*$). A fibre is in the following state according to its shortest embedded length l:

   $L<w_{\max}/2$ the fibre is pulled out,

   $w_{\max}/2<l_N$ the fibre is being pulled out,

   $l_N<L_f/2$ the fibre is debonding,

   where l_N and $w_{\max}$ are the debonding length and the crack opening at the unloading point. From (14), l_N can be related with $w_{\max}$ through:

   $$l_N=\left[\frac{\Delta\tau_N}{\tau}x_{2,N}^2+\frac{d_fE_fw_{\max}}{4(1+\eta)\tau}\right]^{\frac{1}{2}} \tag{35}$$

   Thus, according to Eq. (34), the fibre bridging stress in this period can be calculated through:

   $$\sigma_f(w,N)=\frac{4V_fg_N}{\pi d_f^2L_f^2}\left[\int_{w_{\max}/2}^{l_N}P^{po}(w,N)\,\mathrm{d}L+\int_{l_N}^{L_f/2}P^{db}(w,N)\,\mathrm{d}L\right] \tag{36}$$

   where g_N is the so-called snubbing factor defined in terms of the coefficient f_N as:

   $$g_N=\frac{2}{4+f_N^2}\left(1+\mathrm{e}^{\frac{\pi f_N}{2}}\right) \tag{37}$$

   where f_N is given by (29), P^{po} and P^{db} are forces carried by individual fibres which are in post-debonding and pre-debonding stages, respectively. Replacing P^{po} and P^{db} by the corresponding expressions in different loading states, i.e. first loading, unloading, and

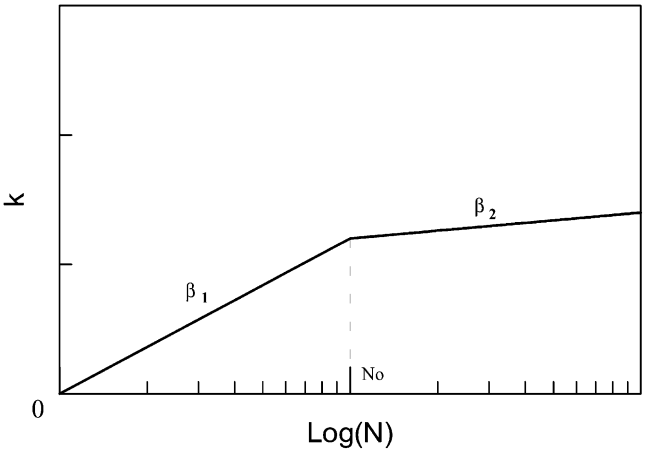

Fig. 6. Bond degradation coefficient k as a function of pull-out cycle N.

reloading (Eqs. (6, 7, 10, 17, 18) and (22)), the bridging stress $\sigma_f(w, N)$ can be obtained by evaluating (36) by numerical integration.

2. After full debonding of all the fibres ($w^* < w_{max} \leq L_f/2$). Similar to the period before full debonding, a fibre is in the following state according to its shortest embedded length L:

   $L < w_{max}$ the fibre is pulled out,

   $w_{max} < L < L_f/2$ the fibre is being pulled out.

   Then, from (34), we have:

$$\sigma_f(w, N) = \frac{4V_f g_N}{\pi d_f^2 L_f^2} \int_{w_{max/2}}^{\frac{L_f}{2}} P^{po}\, dL \tag{38}$$

   Replacing P^{po} with the corresponding expression in different loading states as described above, and integrating (38) numerically, the bridging stress for a certain crack width w and fatigue cycle N in this stage can be solved.

2.1.3. Consideration of Cook-Gordon debonding effect on bridging stress

Li et al. [16] pointed out that an additional bridging compliance as a result of the Cook–Gordon debonding effect has to be included in modelling the relationship between bridging stress and crack width. Cook and Gordon [13] predicted that a crack of finite root radius in an elastic solid under remote tensile load will create a crack tip stress field with a tensile component parallel to the crack plane which reaches a maximum value at the crack tip. Thus a matrix crack approaching an isolated fibre can cause interface debonding before the crack tip reaches the fibre–matrix interface as long as the interfacial strength is adequately weak. This effect will lead to an additional crack opening w_{cg} given by [16]

$$w_{cg} = \frac{4\alpha}{V_f E_f} \sigma_f \tag{39}$$

where α is the debonded length caused by the Cook–Gordon effect which is likely to depend on the inhomogeneity of the interfacial structure [16,19] suggesting that α may lie between $2d_f$ and $10d_f$ for steel fibre in neat cement paste and around $15d_f$ for steel fibre in concrete matrix. When unloading and reloading processes are considered, we assume w_{cg} is a linear function of crack width w and is equal to zero when unloading to w'_{min}, which corresponds to zero bridging stress, i.e.

$$w_{cg} = \frac{w - w'_{min}}{w_{max} - w'_{min}},\ w_{cgm} \tag{40}$$

where w refers to the crack opening at the unloading branch or reloading branch. w_{cgm} is the maximum of the additional crack opening due to the Cook–Gordon effect corresponding to $w = w_{max}$, which can be calculated by (39). Thus the total crack width will be:

$$W = w + w_{cg} \tag{41}$$

2.2. Aggregate bridging behaviour

2.2.1. Monotonic tension

The aggregate bridging in concrete is mainly composed of fine aggregate bridging and coarse aggregate bridging, which are generally governed by the characteristics of aggregates, such as the grading, maximum particle size, surface texture (smooth or rough), and so on. The detailed physics of aggregate bridging in concrete have not been fully understood and a model based on the mechanism of this bridging action has not been developed. Some empirical models of aggregate bridging have been proposed in recent years. In the present investigation, an empirical model proposed by Stang and Aarre [20], which fits a wide range of experimental data extremely well, will be adopted. In this model the aggregate bridging stress σ_a is expressed as a function of the crack with W:

$$\sigma_a = \frac{\sigma_{mu}}{1 + \left(\frac{W}{W_0}\right)^p} \tag{42}$$

where σ_{mu} is the maximum bridging stress due to aggregate action at $W=0$, which is equal to the tensile strength of the material. W_0 is the crack width corresponding to a reduction of the stress carrying capacity to 50% of the tensile strength. p is a shape factor.

2.2.2. Cyclic tension

Aggregate bridging degradation in concrete under single cyclic uniaxial tension has been found and investigated by Gopalaratnam and Shah [21], Reinhardt et al. [22] and Hordijk [23]. Due to the lack of a physical model, the crack bridging law of aggregate under cyclic tension is modelled with the simple assumption that the aggregate bridging degradation with load cycle obeys a linear function of $\log(N)$, i.e.

$$\frac{\sigma_{a,N}}{\sigma_{a,1}} = 1 - d \log(N) \tag{43}$$

where $\sigma_{a,N}$ and $\sigma_{a,1}$ denote bridging stress at the Nth cycle and first cycle respectively, d is the stress degradation factor which reflects the rate of aggregate bridging degradation which can be determined from experiments. As the minimum crack width corresponding to the zero loads, d can be approximately related with the maximum crack width W_{max} by

$$d=d_0+\gamma W_{max} \quad (44)$$

where d_0 is the stress degradation factor at W=0 and γ is the slope of the linear relation of bridging degradation factor d and maximum crack width W_{max}. Through analysis of experimental results of plain concrete under cyclic uniaxial tensile tests, it is found that when d_0=0.08 and γ=4 mm^{-1}, the model predictions can fit the test results reasonably. The comparison between (44) and test results [22] is shown in Fig. 7. If we further assume the aggregate bridging stress linearly reduces with crack closing and the stress reduces to zero as the crack is full closed (W=0), then the unloading branch obeys:

$$\sigma=\sigma_{max}[1-(d_0+\gamma W_{max})\log(N)]\frac{W}{W_{max}} \quad (45)$$

and the reloading branch obeys:

$$\sigma=\sigma_{max}[1-(d_0+\gamma W_{max})\log(N+1)]\frac{W}{W_{max}} \quad (46)$$

σ_{max} is the stress at maximum crack width W_{max} in the first cycle, which is given by (42). The unloading and reloading branches of aggregate bridging are shown in Fig. 8.

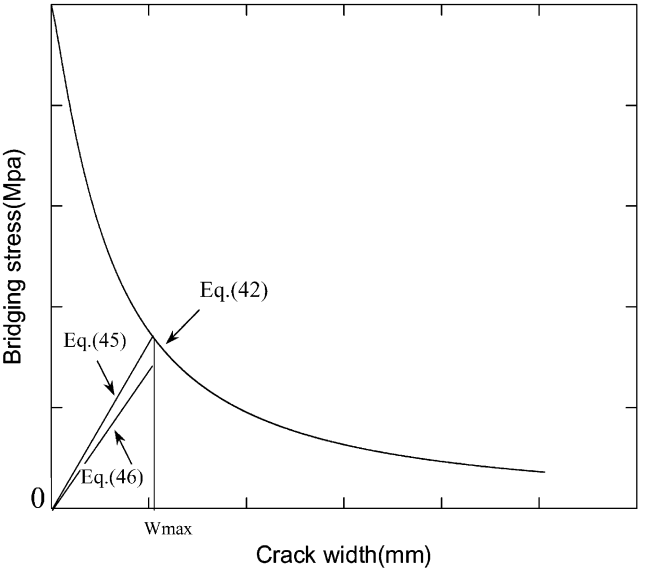

Fig. 8. Aggregate bridging, unloading and reloading paths.

3. Numerical results and experimental verification

3.1. Experimental determination of crack bridging in FRC under uniaxial fatigue tension

In order to verify the present model, a number of uniaxial fatigue tensile tests on straight shaped steel FRC under deformation control are carried out. The mix proportions are given in Table 1. A testing method for measuring the stress–crack width relationship developed by Stang and Aarre [20] is used in the present experimental work and a two-side pre-notched prismatic specimen is adopted. The test set-up and the geometry of the test specimen are shown in Fig. 9. In order to eliminate the pre-stressing inevitably introduced in the specimens when using conventional grips, for improved alignment, and for maximum stiffness, a special specimen fixture was developed. This fixture consisted of two interchangeable steel blocks on which the specimens were glued. The steel blocks were both fixed in advance to the frame and the crosshead of a 250 KN 8500 Instron testing machine. The deformation was measured using two standard Instron extensometers with 12.5 mm gauge length mounted across each of the two 11 mm deep and 3 mm wide notches. Sine waveform with constant maximum and minimum crack width values were used. The load frequency was 3.5 Hz. A series of fatigue tests with different maximum crack width values were conducted. The minimum crack width values were determined by a single cyclic tensile test at which the load equals zero at the unloading branch. A more detailed description of the experiments can be found elsewhere [10,24]. In the present paper, the experimental measurements of the crack bridging under cyclic tension are

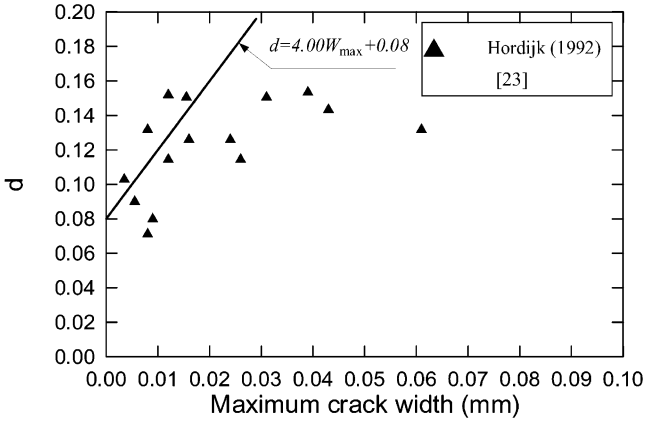

Fig. 7. Aggregate degradation coefficient d as a function maximum crack width.

Table 1
Mix proportions of steel fibre concrete

Ingredients	Dosage (kg/m^3)
Cement	500
Sand (maximum particle size 4 mm)	810
Gravel (maximum particle size 8 mm)	810
Superplasticizer (66% water content)	3.25
Water	237.5
Smooth or hooked steel fibres	78.4
Fibre volume content V_f	1%

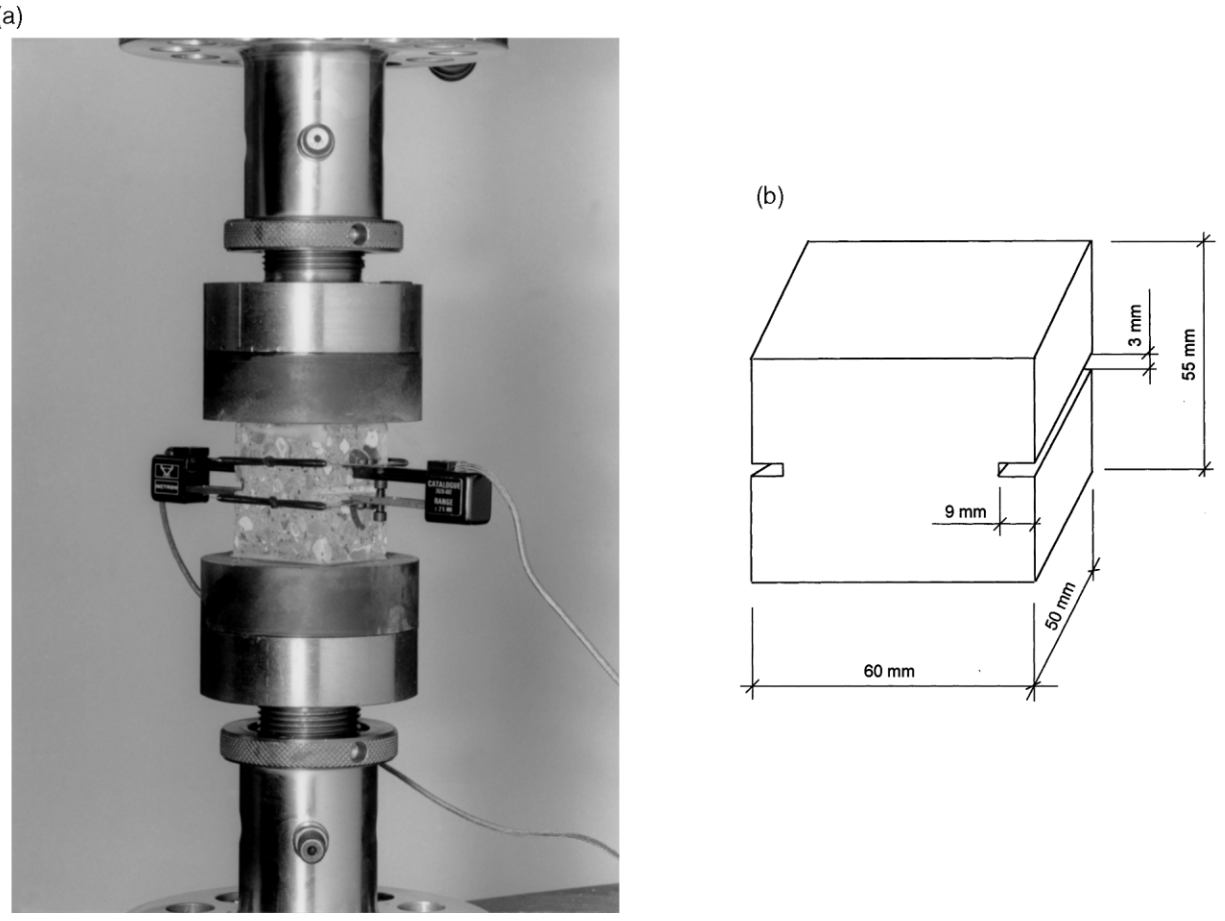

Fig. 9. (a) View of the test set-up for uniaxial tension and (b) the geometry of the specimen.

compared with the model predictions based on independent parametric inputs.

3.2. Parameters for model input

It has been shown that the aggregate bridging model shown by (42) with p=1.2 and W_0=0.015 mm fits a wide range of experimental data extremely well, including normal and high strength concrete [20]. The tensile strength σ_{mu} and Young's modulus E_m were obtained from the direct tensile tests with dog-bone shaped specimens. The matrix related parameters, including matrix bridging degradation parameters d_0 and γ, are given in Table 2.

Without direct fibre pull-out data on this type of matrix, both fibre and matrix used in the present experiments were similar to those used in previous work [16]. The slip-dependent bond parameters used here, as shown in Table 3, are close to the parameters reported in [16]. The snubbing coefficient f, Cook–Gordon parameter α, and fibre parameters, L_f, d_f and E_f, are also given in Table 3.

For the bond degradation parameters, β_1, β_2 and N_0, due to the lack of experimental data of a single fibre under cyclic pull-out load, these parameters were guessed based on the test results of bridging stress degradation, as shown in Table 4.

3.3. Numerical results of crack bridging and comparisons with test results

The crack bridging behaviour of straight steel FRC with 1% volume fraction under fatigue tension with a constant maximum and minimum crack width was

Table 2
Matrix and aggregate bridging parametric value used in model

Name	E_m (GPa)	σ_{mu} (MPa)	p	W_0 (mm)	d_0	γ (mm^{-1})
Values	35	5.42	1.2	0.015	0.08	4

Table 3
Fibre and interfacial parametric value used in model

Name	E_f (GPa)	L_f (mm)	d_f (mm)	τ_0 (MPa)	a_1 (MPa mm^{-1})	a_2 (MPa mm^{-1})	f	α (mm)
Values	210	25	0.4	4.9	−4.5	3.5	0.75	6.0

Table 4
Fibre/matrix interfacial degradation parameters used in model

Name	N_0	β_1 (mm^{-1})	β_2 (mm^{-1})
Values	10	60	10

obtained by numerical calculation using the present semi-analytical model. The analysis was conducted based on the interfacial bond degradation model given by (33), which accounts for both number of load cycles and accumulated fibre slippage amplitude, i.e. the difference between maximum and minimum crack widths. The maximum and minimum crack width values used in the theoretical calculations were all chosen according to the experimental conditions. A total of six series with maximum crack widths of 0.05, 0.10, 0.20, 0.30, 0.40 and 0.50 mm were analysed. The calculated results together with the experimental data are given in Figs. 10–13.

Fig. 10(a) and (b) present the typical loading–unloading loops under deformation controlled uniaxial fatigue tensile load, showing both cases of before full debonding of all fibres and after full debonding of fibres. Fig. 11 shows the computed curves of corresponding bond strength degradation with number of load cycles in these two cases. From Fig. 10, it can be seen that the loading–unloading loops of crack bridging with bond degradation are reproduced successfully by the present model. Fig. 12(a)–(f) shows the predicted relations between maximum bridging stress normalised with respect to the value at the first cycle σ_1 and number of cycles N at maximum crack widths 0.05, 0.10, 0.20, 0.30, 0.40 and 0.50 mm, respectively, shown together with the experimental data obtained from the uniaxial fatigue tensile tests described in Section 3.1. From these results, it can be found that the two-stage degradation law of crack bridging observed in the experiments, a fast dropping stage (about first 10 cycles) followed by a stable decreasing stage, is successfully simulated by the present model. Very good agreement is found in most of the experimental series except for those with small pre-cracked width cases, e.g. W_{max}=0.05 and 0.10 mm. In these two cases, the theoretical results overestimated the cycle-induced degradation effect.

The effect of the maximum crack width on the crack bridging degradation is shown in Fig. 13, where the maximum bridging stress is normalized by the stress at

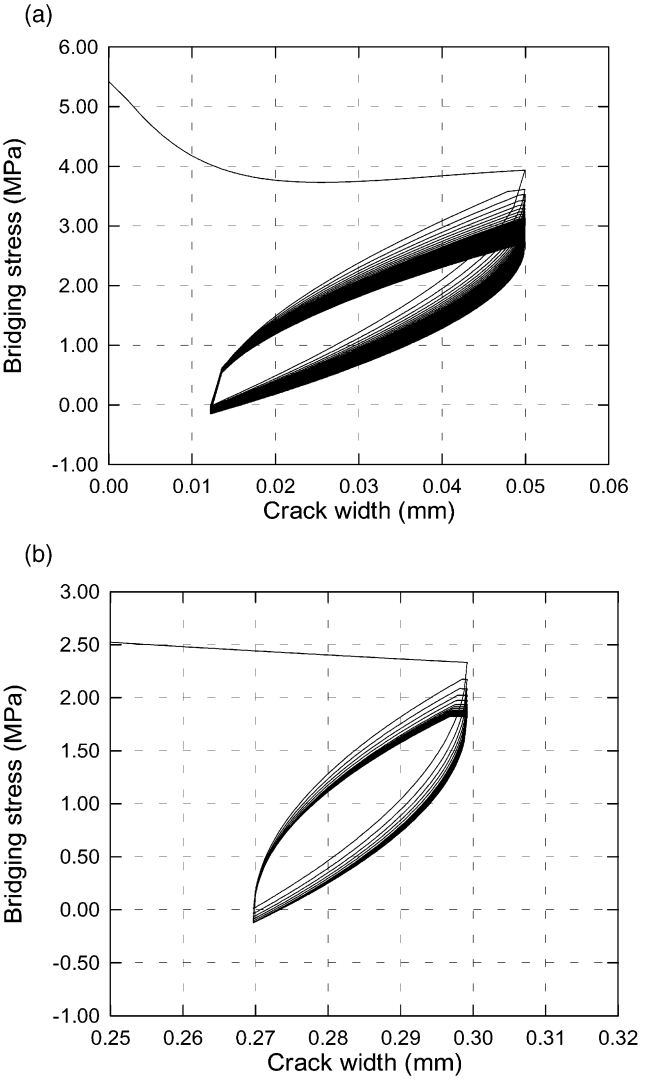

Fig. 10. Load–unload loops of crack bridging under cyclic loading, (a) before full fibre debonding and (b) after full fibre debonding.

the first cycle, comparing both theoretical calculations and experimental data, showing results after 10 and 100 cycles. Due to the aggregate bridging degradation, the normalized bridging stress at zero crack width is not equal to one. From the theoretical predictions, the largest fibre bridging degradation appears at the full fibre debonding point. As the aggregate bridging degradation is included, the total largest bridging degradation will appear around the full fibre debonding point also, but this slightly depends on the aggregate bridging behaviour. Before this peak, the larger the maximum crack

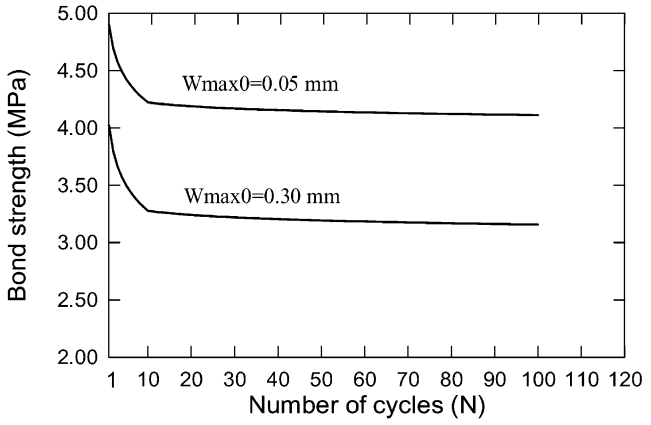

Fig. 11. Typical bond strength degradation with load cycle.

width, the larger the bridging degradation. After that, the case is reversed, i.e. the larger the maximum crack width, the smaller the bridging degradation.

Good agreement is found between model predictions and experimental results. Clearly, as can be seen from Figs. 12 and 13, the theoretical model can effectively capture the key features of crack bridging in FRC under fatigue tension.

4. Conclusions

A micromechanically based semi-analytical model with interfacial bond degradation which describes the crack bridging stress in short randomly oriented fibre reinforced brittle matrix composites under uniaxial cyclic tension has been developed. The loading–unloading loops are successfully reproduced with the present model. Comparisons between model predictions on stress–crack width (σ–W) relationship under fatigue tension and the results of a series of fatigue tensile tests on steel FRC indicates reasonablly good agreement, capturing most of the significant characteristics observed experimentally.

The model is based on the assumption that the bond strength of fibre/matrix and aggregate/fibre interfaces will degrade under cyclic loading. In the present model, apart from monotonic micromechanics parameters, such as matrix parameters (E_m, V_m, σ_m, p, W_0), fibre parameters (E_f, V_f, L_f, d_f) and the fibre/matrix interface parameter, τ, two new parameters, β_1, β_2, used to describe the cyclic fibre/matrix interface degradation rate, are included.

The first application of this model is to evaluate the crack bridging behaviour of different fibre–matrix systems as carried out in this paper. This model can be applied to assess the fatigue performance of composite material structural elements, such as FRC beams and slabs, when suitably combined with a fracture mechanics model. Another potential application of the present model is to serve in the design and optimization of FRC materials with superior fatigue properties. Structural components loaded under cyclic conditions, such as bridge decks, should benefit from such materials.

Acknowledgements

This work has been supported by a grant from the Danish Ministry of Education to the Technical University of Denmark. Support from the National Science Foundation (CMS-9872357) to the University of Michigan and from The Ministry of Education, P.R.C., are acknowledged.

Appendix A. Derivation of debonding stage P–(w, N) relation

Consider an isolated fibre with a round cross section being stretched out from a matrix cylinder by a cyclic force P with a constant amplitude A between maximum and minimum fibre-end slippage values δ_{max} and δ_{min}, corresponding crack openings w_{max} and w_{min}, loads P_{max} and P_{min}, as shown in Fig. 1.

1. First loading stage ($0 \rightarrow \delta_{max}$). In this stage, the debonding zone is gradually extended with the increase in load. Using the strain compatibility requirement at the debonding end (i.e. the axial strain in the fibre ε_f and that in the matrix ε_m are the same) and boundary conditions that $x=l$, $P_m=0$, where P_m is the force in the matrix, the axial force in the fibre and matrix along the debonding length l can be given by:

$$P_f(x)=\eta\pi d_f\tau l+\pi d_f\tau x$$
$$P_m(x)=\pi d_f\tau l-\pi d_f\tau x \quad \text{(A1)}$$

where $\eta \equiv A_fE_f/A_mE_m=V_fE_f/V_mE_m$, and A_f and A_m are the cross-section areas of the fibre and matrix shell, respectively. Thus, the strain distributions in the fibre and matrix along l are:

$$\varepsilon_f(x)=\frac{4\eta\tau l}{d_fE_f}+\frac{4\tau}{d_fE_f}x$$
$$\varepsilon_m(x)=\frac{4\eta\tau l}{d_fE_f}-\frac{4\eta\tau}{d_fE_f}x \quad \text{(A2)}$$

It can be seen that stains in the fibre and matrix are distributed linearly along the debonding length, as the bond strength τ is a constant at any location, as shown in Fig. 2. From (A1), the pull-out force can be expressed as:

$$P=(1+\eta)\pi d_f\tau l \quad \text{(A3)}$$

Again, the relative displacement between fibre and

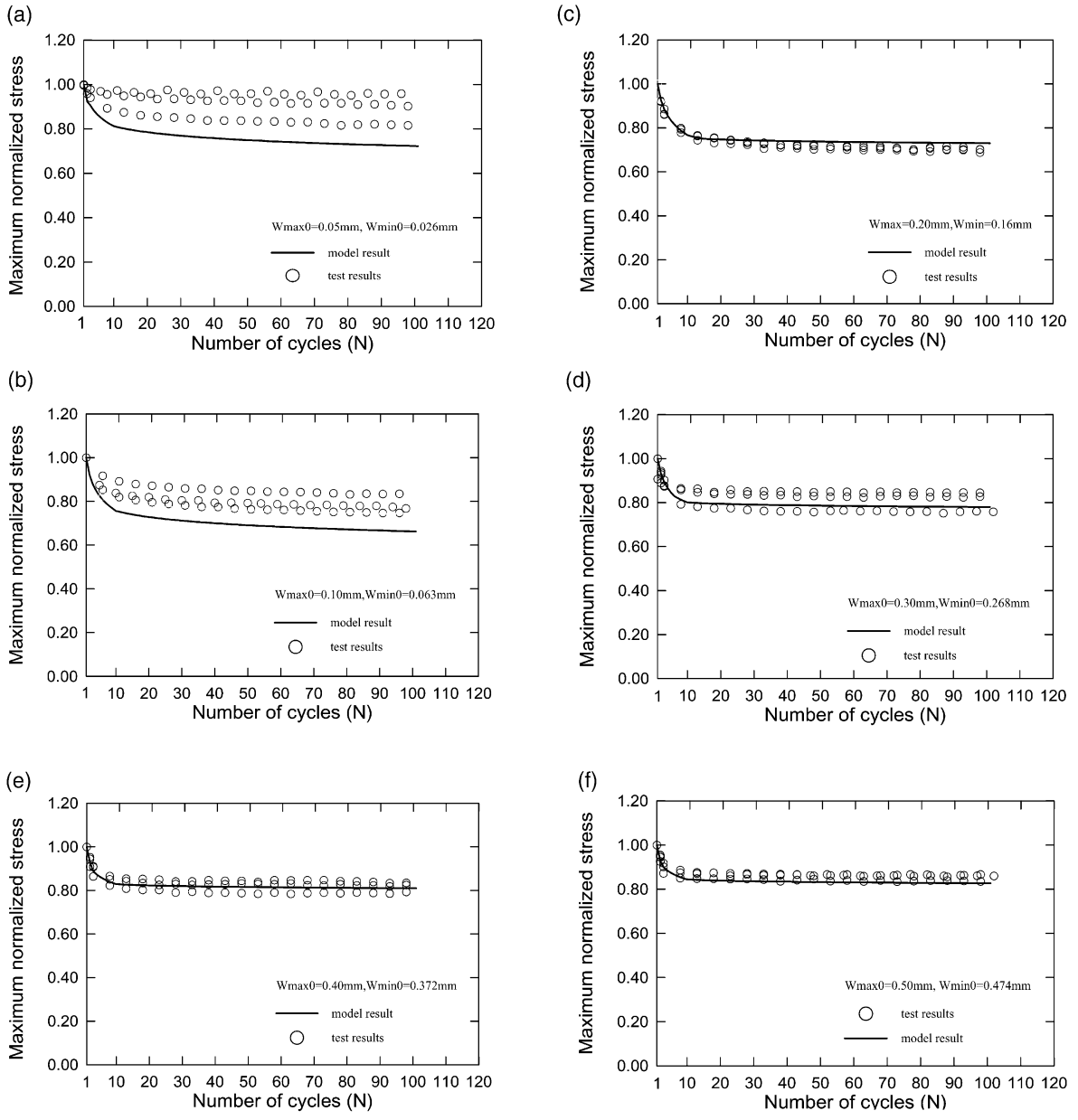

Fig. 12. Maximum normalized bridging stress with load cycle for different maximum pre-cracked values, comparison between theoretical predictions and experimental results.

matrix produces the fibre slippage. Therefore, fibre-end slippage δ can be calculated through:

$$\delta=\int_0^l [\varepsilon_f(x)-\varepsilon_m(x)]\,dx \tag{A4}$$

Replacing $\varepsilon_f(x)$ and $\varepsilon_m(x)$ with (A2) in (A4), we get:

$$l=\left[\frac{d_f E_f \delta}{2\tau(1+\eta)}\right]^{\frac{1}{2}} \tag{A5}$$

Replacing l with (A5) in (A3), the relationship between pull-out load P and fibre-end slippage δ is given as:

$$P(\delta)=\frac{\pi}{\sqrt{2}}[(1+\eta)E_f d_f^3 \tau\delta]^{\frac{1}{2}} \tag{A6}$$

When both segments are considered, we have

$$P(w)=\frac{\pi}{2}[(1+\eta)E_f d_f^3 \tau w]^{\frac{1}{2}} \tag{A7}$$

here $w=2\delta$.

2. Unloading stage ($\delta_{max}\rightarrow\delta_{min}$). Assuming a fibre that has undergone N times of loading–unloading cycles, now it is unloading to P from P_{max}, a reversed zone on bond stress of (l_N-x_1) is created along debonding length l_N and the corresponding bond strengths in the

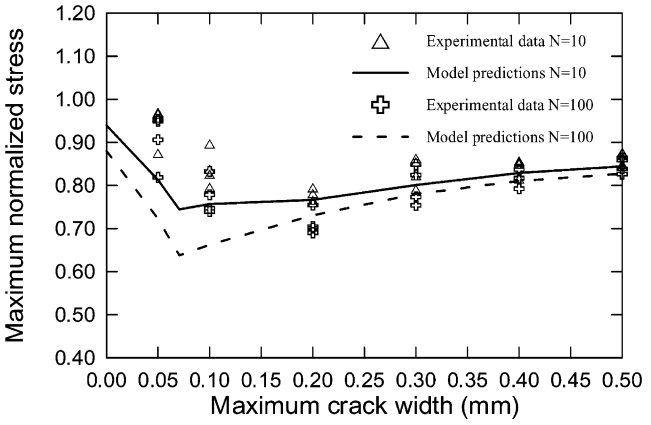

Fig. 13. Effect of maximum pre-cracked width on the bridging degradation, showing together the theoretical and experimental results.

different sections are τ and τ_N, see Fig. 3. The axial force in the fibre along l_N can be given by:

$$P_{f1}(x)=P_{f0}+\pi d_f\tau x(0<x<x_{1,N})$$
$$P_{f2}(x)=P_{f0}+\pi d_f\tau x_{1,N}+\pi d_f\tau_N(x-x_{1,N})(x_{1,N}<x<x_1)$$
$$P_{f3}(x)=P_{f0}+\pi d_f\tau x_{1,N}+\pi d_f\tau_N(x_1-x_{1,N})-\pi d_f\tau_N(x-x_1)(x_1<x<l_N) \quad (A8)$$

where

$$P_{f0}=\eta\pi d_f[\tau x_{1,N}+\tau_N(2x_1-l_N-x_{1,N})] \quad (A9)$$

The axial force in the matrix along l_N can be given by:

$$P_{m1}(x)=P_{m0}-\pi d_f\tau x(0<x<x_{1,N})$$
$$P_{m2}(x)=P_{m0}-\pi d_f\tau x_{1,N}-\pi d_f\tau_N(x-x_{1,N})(x_{1,N}<x<x_1)$$
$$P_{m3}(x)=P_{m0}-\pi d_f\tau x_{1,N}-\pi d_f\tau_N(x_1-x_{1,N})+\pi d_f\tau_N(x-x_1)(x_1<x<l_N) \quad (A10)$$

where

$$p_{m0}=\pi d_f[\tau x_{1,N}+\tau_N(2x_1-l_N-x_{1,N})] \quad (A11)$$

Using condition $x=l_N$ in (A8), the pull-out load P can be expressed as:

$$P=(1+\eta)\pi d_f[\tau_N(2x_1-l_N)+\Delta\tau_N x_{1,N}] \quad (A12)$$

Similar to the first loading stage, the crack width w can be calculated through:

$$w=2\left\{\int_0^{x_{1,N}}[\varepsilon_{f1}(x)-\varepsilon_{m1}(x)]\,dx+\int_{x_{1,N}}^{x_1}[\varepsilon_{f2}(x)-\varepsilon_{m2}(x)]\,dx+\int_{x_1}^{l_N}[\varepsilon_{f3}(x)-\varepsilon_{m3}(x)]\,dx\right\} \quad (A13)$$

Using (A8) and (A10) in (A13), after integration we get

$$w=\frac{4(1+\eta)}{d_fE_f}[\tau l_N^2-(\tau+\tau_N)(l_N-x_1)^2-\Delta\tau_N(x_1-x_{1,N})(2l_N-x_1-x_{1,N})] \quad (A14)$$

Next, from (A14), x_1 can be expressed as:

$$x_1=l_N-\left[\frac{1}{2\tau_N}\left(\tau l_N^2-\frac{d_fE_f}{4(1+\eta)}w-\Delta\tau_N(l_N-x_{1,N})^2\right)\right]^{\frac{1}{2}} \quad (A15)$$

When $P=P_{min}$, $w=w_{min}$ and $x_1=x_{1,N}$, thus from (A15), we have:

$$x_{1,N}=l_N-\left[\frac{\tau}{\tau+\tau_N}l_N^2-\frac{d_fE_f}{4(\tau+\tau_N)(1+\eta)}w_{min}\right]^{\frac{1}{2}} \quad (A16)$$

Then using (A15) and (A16) for x_1 and $x_{1,N}$, respectively, in (A12), the relationship between load P and crack width w and cycle N is obtained.

3. Reloading stage ($\delta_{min}\rightarrow\delta_{max}$). For reloading to P from minimum load P_{min}, the debonding length is divided into three sections, $x_{1,N}$, x_{21} and x_{22}, with bond strengths τ, τ_N and τ_{N+1}, respectively, and specific bond directions, see Fig. 4. Through the same processing procedures as used in the unloading stage, the pull-out force is given by

$$P=(1+\eta)\pi d_f[\tau x_{1,N}+\tau_{N+1}(l_N-x_{1,N})-(\tau_N+\tau_{N+1})x_{21}] \quad (A17)$$

and the crack opening is

$$w=\frac{8(1+\eta)}{d_fE_f}\left[\tau x_{1,N}\left(l_N-\frac{1}{2}x_{1,N}\right)-\tau_N x_{21}\left(l_N-x_{1,N}-\frac{1}{2}x_{21}\right)+\tau_{N+1}\frac{1}{2}(l_N-x_{1,N}-x_{21})^2\right] \quad (A18)$$

In this period, the debonding length l_N is the same as the last cycle. Solving (A18), x_{21} can be expressed as:

$$x_{21}=(l_N-x_{1,N})-\frac{1}{\sqrt{\tau_N+\tau_{N+1}}}\left[\tau_N(l_N-x_{1,N})^2-2\tau x_{1,N}\left(l_N-\frac{1}{2}x_{1,N}\right)+\frac{d_fE_f}{4(1+\eta)}w\right]^{\frac{1}{2}} \quad (A19)$$

Then replacing x_{21} and $x_{1,N}$ with (A19) and (A16) in (A17), we can obtain the expression of reloading level P as a function of w and load cycle N.

As fibres continue to be pulled out after x_{21} becomes zero, the stress degradation zone ($x_{2,N}$) will equal a constant, as shown in Fig. 5, and $x_{2,N}$ can be calculated by the follow formula:

$$x_{2,N}=l_N-x_{1,N} \quad (A20)$$

where $x_{1,N}$ is given by (A16) and l_N is the debonding length of the last cycle. The pull-out force is given by:

$$P=(1+\eta)\pi d_f[\tau(l_{N+1}-x_{2,N})+\tau_{N+1}x_{2,N}] \quad \text{(A21)}$$

In the meantime, the axial force in the fibre and matrix along the debonding length are given by:

$$P_{f1}(x)=P_{f0}+\pi d_f\tau x(0<x\le l_{N+1}-x_{2,N})$$
$$P_{f2}(x)=P_{f0}+\pi d_f\tau(l_{N+1}-x_{2,N})+\pi d_f\tau_{N+1}(x-l_{N+1}+x_{2,N})(l_{N+1}-x_{2,N}<x\le l_{N+1}) \quad \text{(A22)}$$

and

$$P_{m1}(x)=P_{m0}-\pi d_f\tau x(0<x\le l-x_{2,N})$$
$$P_{m2}(x)=P_{m0}-\pi d_f\tau(l-x_{2,N})-\pi d_f\tau_{N+1}(x-l+x_{2,N})(l-x_{2,N}<x\le l) \quad \text{(A23)}$$

Through similar procedures, the crack width w can be expressed as

$$w=\frac{4(1+\eta)}{d_fE_f}[\tau(l_{N+1}-x_{2,N})^2+2\tau x_{2,N}(l_{N+1}-x_{2,N})+\tau_{N+1}x_{2,N}^2] \quad \text{(A24)}$$

Solving l_{N+1} in (A24), we have:

$$l_{N+1}=\left[\frac{\Delta\tau_{N+1}}{\tau}x_{2,N}^2+\frac{d_fE_fw}{4(1+\eta)\tau}\right]^{\frac{1}{2}} \quad \text{(A25)}$$

where $\Delta\tau_{N+1}=\tau-\tau_{N+1}$. Equation (A25) is used to calculate the debonding length for a given crack opening and bond strength and loading cycles. Replacing l_{N+1} with (A25) in (A21), we have:

$$P(w,N)=(1+\eta)\pi d_f\tau x_{2,N}\left[\left(\frac{E_fd_fw}{4(1+\eta)\tau x_{2,N}^2}+\frac{\Delta\tau_{N+1}}{\tau}\right)^{\frac{1}{2}}-\frac{\Delta\tau_{N+1}}{\tau}\right] \quad \text{(A26)}$$

Appendix B. Derivation of pull-out stage P–(w, N) relation

1. First loading case ($0\rightarrow\delta_{max}$). In this period, the pull-out load can be approximated related to crack opening by [16] (see Fig. 1(b)):

$$P(\delta)=(1+\eta)\pi d_f\tau(L-\delta+\delta_{fd}) \quad \text{(B1)}$$

where L is the maximum embedded length. When both segments are considered ($\delta=w-\delta_{fd}$), we have:

$$P(w)=(1+\eta)\pi d_f\tau(L-w+w_{fd}) \quad \text{(B2)}$$

where w_{fd} is the crack width at full debonding point of the fibre and $w_{fd}=2\delta_{fd}=4L^2\tau/[(1+\eta)E_fd_f$. During this stage, the matrix will try to keep the strain level at the bonded end of the fibre. Therefore, the strain compatibility condition at this fibre end is still valid. Thus, the distribution of axial force and strain in fibre and matrix along the embedded length l ($l=L-w+w_{fd}$) in this stage can still be expressed as those in the debonding stage.

2. Unloading case ($\delta_{max}\rightarrow\delta_{min}$). Similar to the debonding case, assuming that a fibre in the pull-out stage that has undergone N times of loading–unloading cycles, now is unloading to P from P_{max}, a reversed zone on the bond stress of (l_N-x_1) is created along the embedded length l_N and the corresponding bond strength in the different sections are τ and τ_N. According to the fact described above, the pull-out load P can still be given by (A13). But the fibre exit–end slippage will include the pull-out value at the other fibre end besides the slippage due to the bond between the fibre and the matrix (see Fig. 1). Thus, the resulting crack opening is:

$$w=2\left\{\int_0^{x_{1,N}}[\varepsilon_{f1}(x)-\varepsilon_{m1}(x)]\,dx+\int_{x_{1,N}}^{x_1}[\varepsilon_{f2}(x)-\varepsilon_{m2}(x)]\,dx+\int_{x_1}^{^1N}[\varepsilon_{f3}(x)-\varepsilon_{m3}(x)]\,dx\right\}+w_{max}-w_{fdN} \quad \text{(B3)}$$

where $l_N=L-w_{max}+w_{fdN}$. ($w_{max}-w_{fdN}$) is the permanent pull-out value at the other fibre end at cycle N and w_{fdNl} can be given by:

$$w_{fdN}=\frac{4(1+\eta)}{d_fE_f}[\tau L^2-\Delta\tau_{N-1}(L-x_{1,N-1})] \quad \text{(B4)}$$

Using the same expressions of axial force in fibre and matrix shown in the fibre debonding stage in (B3), we obtain:

$$w=\frac{4(1+\eta)}{d_fE_f}[\tau l_N^2-(\tau+\tau_N)(l_N-x_1)^2-\Delta\tau_N(x_1-x_{1,N})(2l_N-x_1-x_{1,N})]+w_{max}-w_{fdN} \quad \text{(B5)}$$

As for the fibre debonding case, x_1 and $x_{1,N}$ can be expressed as:

$$x_1=l_N-\left[\frac{1}{2\tau_N}\left(\tau l_N^2-\frac{d_fE_f}{4(1+\eta)}(w-w_{max}+w_{fdN})-\Delta\tau_N(l_N-x_{1,N})^2\right)\right]^{\frac{1}{2}} \quad \text{(B6)}$$

and

$$x_{1,N}=l_N-\left[\frac{\tau}{\tau+\tau_N}l_N^2-\frac{d_fE_f}{4(\tau+\tau_N)(1+\eta)}(w_{min}-w_{max}+w_{fdN})\right]^{\frac{1}{2}} \quad \text{(B7)}$$

Then replacing x_1 and $x_{1,N}$ with (B6) and (B7) in (A12), the relationship of unloading level P and crack width w and number of cycles N during this fibre pull-out stage is obtained.

3. Reloading case ($\delta_{\min} \rightarrow \delta_{\max}$). Reloading to P from minimum load $P_{\min}$, using the same procedures used in the fibre debonding period and paying attention to the differences in the crack opening components in fibre debonding and pull-out stages, the second reversed zone x_{21} can be expressed as:

$$x_{21}=(l_N-x_{1,N})-\frac{1}{\sqrt{\tau_N+\tau_{N+1}}}\left[\tau_N(l_N-x_{1,N})^2 -2\tau x_{1,N}\left(l_N-\frac{1}{2}x_{1,N}\right)+\frac{d_f E_f}{4(1+\eta)}(w-w_{\max}+w_{fdN})\right]^{\frac{1}{2}} \quad \text{(B8)}$$

Replacing x_{21} with (B8) in (A17), we obtain the relationship of reloading level P, crack width w and number of cycles N.

As in the debonding period, when the fibre is continuing to be pulled out, as shown in Fig. 5, the bridging force can be given by:

$$\begin{aligned} P&=(1+\eta)\pi d_f[\tau_{N+1}(L-w+w_{fdN})+\Delta\tau_{N+1}x_{1,N}] && \text{for } w\le l_N-x_{1,N}+w_{\max}\\ P&=(1+\eta)\pi d_f\tau(x_{1,N}-w+w_{fdN}) && \text{for } \delta>l_N-x_{1,N}+w_{\max} \end{aligned} \quad \text{(B9)}$$

where $l_N=L-w_{\max}+w_{fdN}$.

References

[1] Ramakrishan V, Oberling G. Performance characteristics and fatigue strength of polypropylene fibre reinforced concrete. SP-105. Detroit (MI): America Concrete Institute, 1987:225–45.

[2] Otter DE, Naaman AE. Properties of steel fibre reinforced concrete under cyclic loading. ACI Mater J 1988;85(4):254–61.

[3] Grzybowski M, Meyer C. Damage accumulation in concrete with and without fibre reinforcement. ACI Mater J 1993;90(6):594–604.

[4] Zhang J, Stang H. Fatigue performance in flexure of fibre reinforced concrete. ACI Mater J 1998;95(1):58–67.

[5] Li VC, Matsumoto T. Fatigue crack growth analysis of fibre reinforced concrete with effect of interfacial bond degradation. Cement Concrete Composites 1998;20(5):353–63.

[6] Cox BN, Rose LRF. Time- or cycle-dependent crack bridging. Mech Mater 1994;19:39–57.

[7] Evans AG, Zok FW, Mcmeeking RM. Fatigue of ceramic matrix composites. Acta Metall Mater 1995;43(3):859–75.

[8] Zhang J, Stang H, Li VC. Fatigue life prediction of fiber reinforced concrete under flexural load. Int J Fatigue 1999;21(10):1033–49.

[9] Zhang J, Stang H. Interfacial degradation in cement-based fibre reinforced composites. J Mater Sci Lett 1997;16(11):886–8.

[10] Zhang J, Stang H, Li VC. Experimental study on crack bridging in FRC under uniaxial fatigue tension. ASCE J Mater Civil Engng 2000;12(1):66–73.

[11] Wu HC, Matsumoto T, Li VC. Bucking of bridging fibres in composites. J Mater Sci Lett 1994;13(24):1800–3.

[12] Li VC, Wang Y, Backer S. Effect of inclining angle, bundling, and surface treatment on synthetic fibre pull-out from a cement matrix. Composites 1990;21(2):132–40.

[13] Cook J, Gordon JE. A mechanism for the control of crack propagation in all brittle systems. Proc Roy Soc 1964;282A:508–20.

[14] Wang Y, Li VC, Backer S. Modeling of fiber pull-out from a cement matrix. Int J Cem Compos Lightwt Concr 1988;10(3):143–9.

[15] Aarre T. Tensile characteristics of FRC with special emphasis on its applicability in a continuous pavement. PhD thesis, Department of Structural Engineering and Materials, Technical University of Denmark, 1992 [Series R, No. 301].

[16] Li VC, Stang H, Krenchel H. Micromechanics of crack bridging in fibre-reinforced concrete. Mater Struct 1993;26:486–94.

[17] Morton J, Groves GW. The cracking of composites consisting of discontinuous ductile fibres in a brittle matrix — effect of fibre orientation. J Mater Sci 1974;9(9):1436–45.

[18] Li VC, Wang Y, Backer S. A micromechanical model of tension softening and bridging toughening of short random fibre reinforced brittle matrix composites. J Mech Phys Solids 1991;39(5):605–25.

[19] Bentur A, Diamond S, Mindess S. Cracking process in steel fibre reinforced cement paste. Cement Concrete Res 1985;15(2):331–42.

[20] Stang H, Aarre T. Evaluation of crack width in FRC with conventional reinforcement. Cement Concrete Composites 1992;14(2):143–54.

[21] Gopalaratnam VS, Shah SP. Softening response of plain concrete in direct tension. ACI J 1985;82(3):310–23.

[22] Reinhardt HW, Cornelissen AW, Hordijk DA. Tensile tests and failure analysis of concrete. J Struct Engng 1986;112(11):2462–77.

[23] Hordijk DA. Tensile and tensile fatigue behaviour of concrete, experiments, modelling and analyses. HERON 1992;37(1).

[24] Zhang J. Fatigue fracture of fiber reinforced concrete — an experimental and theoretical study. Ph.D thesis, Department of Structural Engineering and Materials, Technical University of Denmark, 1998 [Series R, No. 41].